frontiers | Frontiers in Energy Research

TYPE Original Research
PUBLISHED 04 October 2022
DOI 10.3389/fenrg.2022.970293

Check for updates

OPEN ACCESS

EDITED BY
Umar Khan,
Hazara University, Pakistan

REVIEWED BY
Basharat Ullah,
Mohi-Ud-Din Islamic University, Pakistan
Muhammad Farooq,
University of Engineering and Technology, Lahore, Pakistan
Zulqurnain Sabir,
United Arab Emirates University, United Arab Emirates

*CORRESPONDENCE
Elsayed Tag Eldin,
Elsayed.tageldin@fue.edu.eg

SPECIALTY SECTION
This article was submitted to Process and Energy Systems Engineering, a section of the journal Frontiers in Energy Research

RECEIVED 15 June 2022
ACCEPTED 01 August 2022
PUBLISHED 04 October 2022

CITATION
Gul T, Mukhtar S, Alghamdi W, Tag Eldin E, Yassen MF and Guedri K (2022), The radiative flow of the thin-film Maxwell hybrid nanofluids on an inclined plane in a porous space. *Front. Energy Res.* 10:970293.
doi: 10.3389/fenrg.2022.970293

The radiative flow of the thin-film Maxwell hybrid nanofluids on an inclined plane in a porous space

Taza Gul[1], Safyan Mukhtar[2], Wajdi Alghamdi[3], Elsayed Tag Eldin[4]*, Mansour F. Yassen[5,6] and Kamel Guedri[7]

[1]Department of Mathematics, City University of Science and Information Technology, Peshawar, Pakistan, [2]Department of Basic Sciences, Deanship of Preparatory Year, King Faisal University, Hafuf, Al Ahsa, Saudi Arabia, [3]Department of Information Technology, Faculty of Computing and Information Technology, King Abdulaziz University, Jeddah, Saudi Arabia, [4]Faculty of Engineering and Technology, Future University in Egypt New Cairo, Cairo, Egypt, [5]Department of Mathematics, College of Science and Humanities in Al-Aflaj, Prince Sattam Bin Abdulaziz University, Al-Aflaj, Saudi Arabia, [6]Department of Mathematics, Faculty of Science, Damietta University, Damietta, New Damietta, Egypt, [7]Mechanical Engineering Department, College of Engineering and Islamic Architecture, Umm Al-Qura University, Makkah, Saudi Arabia

Due to their accelerated rate of heat transfer, nanofluids are of immense interest. This work analyzes an innovative concept of hybrid nanoemulsion with an optimized design under the chemical radiative flow and its thermophysical properties. We are able to achieve great aspects of the flow with the assistance of the sheet's permeable texture and inclined surface. Furthermore, the effects of thermal conductivity mix convection, chemical reaction, and thermal radiations on velocity, temperature, and concentration fields are also investigated. After converting the fundamental equations to ordinary differential equations with the use of similarity transportation, the problem is then solved analytically with the HAM technique. To investigate key attributes and parameters, a hybrid nanofluid with Ag and Al_2O_3 nanoparticles as well as Al_2O_3 for conventional nanofluids with the base solvent water is taken. To illustrate the effects of chemical radiative and mix convection on the thin-film flow, numerous graphs, charts, and tables are shown. Calculations and reviews are performed for reduced friction coefficient, heat, and mass transportation. According to this study, hybrid nanofluids have a higher heat-transfer rate than nanofluids when exposed to thermal radiation and at the appropriate surface angle of inclination. Due to $\phi_{Al_2O_3}$, ϕ_{Ag}, S, Rd, the temperature increases, but velocity has the opposite effect. This investigation's innovative findings will promote the study of condensed nanostructures and nanomaterials.

KEYWORDS

Maxwell hybrid nanofluid, thin film, heat and mass transfer, inclined stretching sheet, MgO and TiO_2

Introduction

Table 1 shows the thermophysical properties of the materials. It is common practice to utilize the power-law model when modeling the flow of fluids that have a viscosity that varies with shear. On the other hand, it is not possible to forecast the results of elasticity. Fluids of the second or third grade have the potential to produce the desired outcomes in terms of elasticity. However, in these models, the viscosity is not shear-dependent. Furthermore, they are impotent to assess the effects of reducing stress. A subcategory of fluids known as the Maxwell model, which has become more popular, can identify stress relaxation. A perfectly viscous obstruction and a strictly elastic spring can be represented, much like in the Maxwell model. Maxwell nanofluid flow simulations have drawn the attention of numerous researchers. Abro et al. (2020), Sharama et al. (2020), and Ramesh et al. (2020) have used various mathematical models for the Maxwell fluid flow. The influence of radiative heat flux on the flow of Maxwell nanofluids across a chemically reacting spiraling disc was analyzed by Ahmed et al. (2020). Hussain et al. (2020) took into consideration the mathematical analysis of a Maxwell nanofluid with hydromagnetic dissipative and radiation. Jawad et al. (2021) have analyzed the entropy impact on the flow of Maxwell fluids using stretched surfaces.

The most appealing and affordable method of thermal transportation was proposed by the revolutionary advancement in science using the concept of nanoparticles. Researchers are constantly examining the thermal characteristics of nanoparticles related to engineering and manufacturing usages because they have the highest proficiency of thermal transportation and stable forceful features. The formation of nanofluids is caused by the dispersion of nanoparticles in the base solvent. Plications for nanofluids are anticipated in a variety of fields, including nuclear engineering, mechanical and cooling devices, extrusion systems, and many others. In recent years, the role of nanofluids in energy production has moved into more essential applications. When nanoparticles are adequately dissolved in the base fluid, it is expected that mass and heat transmission will improve. Nanofluids are widely used in biotechnology, medicine delivery, renewable energy, and several technical fields. Choi (1995) coordinated the basic analysis and experimental investigation of the nanofluid characteristics. The thermal measurements of a nanofluid containing micropolar material were described by Khan et al. (2020) using modified diffusion concepts. Khan et al. (2019) have depicted the Oldroyd-B nanofluid flow using the optimal Prandtl number technique. Turkyilmazoglu (2020) used the single-phase model to declare the stability of nanofluids. The impact of porous space over moving surfaces susceptible to the Jeffrey nanofluid was determined by Khan and Shehzad (2020). The dual solution prediction for the nanofluid flow subject to asymmetrical slip was observed by Nadeem et al. (2020). Some other researchers have proposed different forms of nanofluids to study the many uses of nanofluids in various aspects (Sabir et al., 2019; Umar et al., 2020; Ayub et al., 2021a; Ayub et al., 2021b; Sabir et al., 2021).

As an alternative to conventional fluids, nanofluids are renowned for their exceptional capacity to transport energy. In order to make it significantly better, the hybrid nanoliquid is being produced. When two or more types of metals are combined in such a way as to produce different chemical bonds, the resulting substances are referred to be hybrid metals. A "hybrid nanofluid" can also be created by the uniform dispersion of two very small particles into the liquid that is acting as the mother liquid. Comparing this highly developed type of solution to unitary nanofluids or any other common functional fluids, it shows promising heat transmission. The innovative uses for hybrid nanosolutions include the fabrication of aviation devices, power systems, welding, lubricants, spacecraft, and electronic cooling devices. The influence of the magnetic field in the transverse direction to the flow field is discussed by Devi and Devi (2016). Babar and Ali (2019) discussed the specific thermophysical environment, applications, setup, and inherent issues of hybrid composites. Recently, more studies about hybrid nanofluid flow through various configurations can be decoded in Acharya et al. (2020), Yaseen et al. (2022), and Joshi et al. (2022).

The transportation of liquids in thin layers is frequently seen in daily life; one illustration of this is the way raindrops move across rooftops, road surfaces, and window glass. Understanding the process of thin films is crucial since they frequently occur in nature and have numerous useful applications. Whether there are inertial forces present or absent, thin films of liquids are driven by surface or body forces. Depending on the flow pattern under consideration, the strength of these forces acting on the fluid may be increased or decreased. In situations like dropping films or spray coating, inertia is crucial, but it is sometimes disregarded when the flow Reynolds number is low, as in the flow motion over an inclined plane in a sluggish motion. Thin-film flows have drawn a great deal of interest in recent years. Photovoltaic panels, lamination, biofluid flows, hydrophilicity, and other commercial and technical applications all involve film flowing over stirring flat, vertical, and inclined planes (Liu et al., 2017). The first person to look at the case of the dropping liquid films was Nusselt (1916). Jeffrey (1925) also explored the film flow in the scenario of an inclined plane. There are a lot of research studies on film flow on diverse models, which may be found in the Refs. Wang, 1990; Qasim et al., 2016; Zhang et al., 2021; Shah et al., 2022.

The radiation impact plays an important role in almost all the design approaches. Thermal radiation plays a significant role in a variety of mechanical processes, such as missiles, nuclear power plants, spacecraft and other communications satellites, steam turbines, and the many driving mechanisms for aviation. In addition to radiation, Ghadikolaei et al. (2018) and Ali et al. (2020) focused on the thermal radioactive effects in addition to the transfer of nanofluids when studying peristaltic pressing. CuO-Ag/water micropolar hybrid nanofluid flow across a vertically positioned plate was studied by Gumber et al. (2022) with the help of heat radiation and the suction/injection mechanism.

The possibilities for higher thermal transport illustrate the knowledge of the existing literature. Recent investigations of unsteady thin-film flow impacted by advanced ablation/accretion (Wang, 1990; Qasim et al., 2016; Zhang et al., 2021; Shah et al., 2022) address conventional heat transmission modes. We focused on expanding such work to include the chemical radiative effect and the mix convectional characteristics of Maxwell hybrid nanofluid flow. The cited works mentioned aforesaid highlight that less attention is paid to the study of nanofluid flow impressions over an inclined stretched plane keeping insight of Maxwell fluid flow. Nevertheless, the flow of the hybrid nanofluid in the same context is rare. We in this exploration discussed the hybrid nanofluid flow comprising silver with aluminum oxide, nanocomposites, and thin-film flow over an inclined plane. The thermal effects of the nanocomposites are also taken into account in the presence of radiation. The composite factor of the particles plays a significant role in thermal conduction. The film width along with the applied magnetic field has been studied additionally in the graphical form by using the HAM method. The impression of varied parameters versus involved profiles is studied logically.

The following are some of the innovative aspects of this work:

- Due to the intensive use of both laboratory and computational studies, the novel heat-transfer fluid is focused on the appropriate Maxwell fluid-based Al_2O_3-Ag-hybrid nanofluid.
- To explore the heat-transfer phenomenon, a thin film of Maxwell hybrid nanofluid flow on an inclined extended surface using thermal conductivity models has been used.
- To find an analytical solution for heat-transfer effects in hybrid nanofluid flow with thermal radiation, chemical reaction, porosity, and mix convection present.
- The governing equations for heat, mass transport, and fluid motion are transformed into self-similar differential equations using the standard factors, and the HAM method is then used to evaluate them analytically.
- The results are represented in diagrams that correspond to various numeric values of the relevant parameters.

Chemical radiative and convectional heat exchange between the surface and the surrounding fluid is essential in many real-world applications involving the cooling or heating of surfaces.

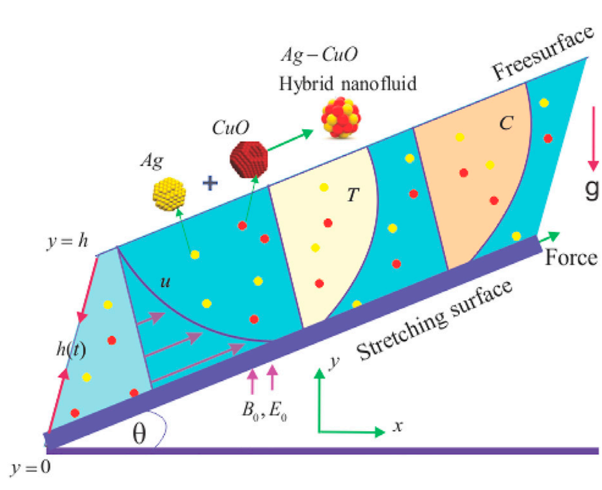

FIGURE 1
Physical sketch of the proposed model.

The problem is more realistic and produces better results because of its cumulative proportion.

Problem development and the governing model

Let us examine the improvement of energy and mass transformation in time-dependent thin-film flow of Maxwell fluids with hybrid and mononanoparticles. Over an extended inclined plane making an angle θ with the surface, a thin film flows. The following considerations are made while modeling the transportation of mass and heat:

1 The surface over which the thin film exists is moving with velocity $U = bx(1-\alpha t)^{-0.5}$; here, the operative elasticity of the velocity is $b(1-\alpha t)^{\frac{-1}{2}}$ toward the x-axis, where "α" signifies the increment of time $(0 \le \alpha < 1)$ and "b" represents the elasticity.
2 The surface temperature of the extending sheet is signified as "T_s", and the temperatures of the slit are defined as T_0 and T_r .The range of these constraints is referred to as $0 \le T_r \le T_0$.
3$\frac{xU_w}{\upsilon} = \frac{bx^2(1-\alpha t)^{-1}}{\upsilon}$ is the local Reynolds number dependent on U_w.
4 h(t) represents the thickness of the film.
5 We consider pressure to be constant.
6 The nanoparticles Al_2O_3 and Ag are used.
7 The magnetic field in a perpendicular direction is defined as $B_0(x,t) = (1-\alpha t)^{\frac{-1}{2}} B_0$.
8.8 The flow configuration for the problem is shown in Figure 1.

The fundamental equations for boundary layers that govern flow, heat, and mass transfer have the following forms (Jawad et al., 2021; Acharya et al., 2020; Zhang et al., 2021; Shah et al., 2022; Gumber et al., 2022):

$$\frac{\partial u}{\partial x}+\frac{\partial v}{\partial y}=0 \tag{1}$$

$$\begin{aligned}\left(\frac{\partial u}{\partial t}+u\frac{\partial u}{\partial x}+v\frac{\partial u}{\partial y}\right) &= \upsilon_{hnf}\frac{\partial^2 u}{\partial y^2}-\lambda_1\left(2uv\frac{\partial^2 u}{\partial x\partial y}+u^2\frac{\partial^2 u}{\partial x^2}+v^2\frac{\partial^2 u}{\partial y^2}\right)\\ &-\left[\frac{\upsilon_{hnf}}{k^{\oplus}}\left(\lambda_1 v\frac{\partial u}{\partial y}+u\right)+\frac{\sigma_{hnf}}{\rho_{hnf}}\left(B^2(x,t)\left(\lambda_1 v\frac{\partial u}{\partial y}+u\right)-E_0B(x,t)\right)\right]\\ &+g\left\{\pm\,(T-T_h)(\beta_T)_{hnf}+(C-C_h)(\beta_C)_{hnf}\right\}Sin\,\theta,\end{aligned} \tag{2}$$

$$\frac{\partial T}{\partial t}+u\frac{\partial T}{\partial x}+v\frac{\partial T}{\partial y}=\alpha_{hnf}\left[\frac{\partial^2 T}{\partial y^2}\right]+\frac{16\sigma^* T_h^3}{3k^*(\rho Cp)_{hnf}}\frac{\partial^2 T}{\partial y^2} \tag{3}$$

$$\frac{\partial C}{\partial t}+u\frac{\partial C}{\partial x}+v\frac{\partial C}{\partial y}=D_{Bhnf}\frac{\partial^2 C}{\partial y^2}-Kr(C-C_h) \tag{4}$$

The components of velocity are represented by u, v and act along x, y directions, respectively; λ_1 is the Maxwell relaxation time parameter (note that for $\lambda_1 = 0$, the problems reduce to the case of classical heat and mass transport of Newtonian fluids); $k^{\oplus}$ is the permeability of the porous medium; β_T, β_C are the coefficients of linear thermal and concentration expansion, respectively; σ^* is the Stefan–Boltzmann constant; k^* is the coefficient of mean absorption; D_{Bhnf} is the diffusion coefficient of the hybrid nanofluid; and Kr is the chemical reaction. Also, the σ_{hnf} (electrical conductivity), μ_{hnf} (dynamic viscosity), ρ_{hnf} (density), $(\rho c_p)_{hnf}$ (capacity of specific heat), and k_{hnf} (thermal conductivity) are some of the hybrid nanofluid quantities that can be described in this way (Acharya et al., 2020 and Joshi et al., 2022).

$$\frac{\mu_{hnf}}{\mu_f}=\frac{\left(1-\phi_{Ag}\right)^{-2.5}}{\left(1-\phi_{Al_2O_3}\right)^{2.5}},\quad \frac{\mu_{nf}}{\mu_f}=\left(1-\phi_{Al_2O_3}\right)^{-2.5} \tag{5}$$

$$\left.\begin{aligned}\frac{\rho_{hnf}}{\rho_f}&=\left(1-\phi_{Al_2O_3}\right)\left(1-\phi_{Ag}\right)+\phi_{Al_2O_3}\left(1-\phi_{Ag}\right)\frac{\rho_{Ag}}{\rho_f}+\phi_{Ag}\frac{\rho_{Al_2O_3}}{\rho_f}\\ \frac{\rho_{nf}}{\rho_f}&=\left(1-\phi_{Al_2O_3}\right)+\phi_{Al_2O_3}\frac{\rho_{Al_2O_3}}{\rho_f}\end{aligned}\right\} \tag{6}$$

$$\left.\begin{aligned}\frac{(\rho c_p)_{hnf}}{(\rho c_p)_f}&=\left(1-\phi_{Ag}\right)\left(1-\phi_{Al_2O_3}\right)+\left(1-\phi_{Ag}\right)\phi_{Al_2O_3}\left(\rho c_p\right)_{Ag}+\phi_{Ag}\left(\rho c_p\right)_{Al_2O_3}\\ \frac{(\rho c_p)_{nf}}{(\rho c_p)_f}&=\left(1-\phi_{Al_2O_3}\right)+\frac{(\rho c_p)_{Al_2O_3}}{(\rho c_p)_f}\phi_{Al_2O_3}\end{aligned}\right\} \tag{7}$$

$$\left.\begin{aligned}\frac{k_{hnf}}{k_{nf}}&=\left(1-\phi_{Ag}\right)+2\left(\frac{k_{Al_2O_3}}{k_{Al_2O_3}-k_{nf}}\right)k_{Ag}\log_e\left(\frac{k_{Al_2O_3}+k_{nf}}{k_{nf}}\right)\\ \frac{k_{nf}}{k_f}&=\left(1-\phi_{Al_2O_3}\right)+2\left(\frac{k_{Ag}}{k_{Ag}-k_{nf}}\right)k_{Al_2O_3}\log_e\left(\frac{k_{Ag}+k_{nf}}{k_{nf}}\right)\end{aligned}\right\} \tag{8}$$

$$\frac{\sigma_{hnf}}{\sigma_f}=1+\frac{3\,\phi_{Al_2O_3}\,\sigma_{Al_2O_3}+3\,\phi_{Ag}\sigma_{Ag}-3\,\phi\,\sigma_f}{\sigma_f\,(2+\phi)+\left(1-\phi_{Al_2O_3}\right)\sigma_{Al_2O_3}+\left(1-\phi_{Ag}\right)\sigma_{Ag}} \tag{9}$$

Therefore, we assumed the composition of Ag into Al_2O_3/H_2O; in the proposed investigation, a hybrid nanofluid was developed. Al_2O_3 nanoparticles ($\phi_{Al_2O_3}$) are first dispersed in H_2O to make a Al_2O_3/H_2O ordinary nanofluid, and then Ag nanomaterials of diverse ratios (ϕ_{Ag}) are mixed to make a consistent hybrid nanofluid of Al_2O_3-Ag/H_2O. We assume that $\phi = \phi_{Al_2O_3} + \phi_{Ag}$ throughout the study.

The physical conditions for the thin-film flow are defined as

$$\left\{\begin{aligned}&u|_{y=0}=U_w,\ v|_{y=0}=0,\mu_{hnf}\left.\frac{\partial u}{\partial y}\right|_{y=h(t)},v=\left.\frac{\partial h}{\partial t}\right|_{y=h(t)},\\ &T|_{y=0}=T_w,\ C|_{y=0}=C_w,\left.\frac{\partial T}{\partial y}\right|_{y=h(t)}=\left.\frac{\partial C}{\partial y}\right|_{y=h(t)}=0.\end{aligned}\right\} \tag{10}$$

The non-dimensional variables and coordinates that we present are as follows (Zhang et al., 2021; Shah et al., 2022):

$$\left.\begin{aligned}&\psi=\left(\frac{bv}{1-\alpha t}\right)^{\frac{1}{2}}xf(\eta),\quad \eta=\left(\frac{b}{\upsilon(1-\alpha t)}\right)^{\frac{1}{2}}y,\\ &T=T_0-T_r\left(\frac{bx^2}{2\upsilon}\right)\frac{\Theta(\eta)}{(1-\alpha t)^{\frac{3}{2}}},C=C_0-C_r\left(\frac{bx^2}{2\upsilon}\right)\frac{\Phi(\eta)}{(1-\alpha t)^{\frac{3}{2}}}.\end{aligned}\right\} \tag{11}$$

where

$$u=\frac{\partial\psi}{\partial y},\quad v=-\frac{\partial\psi}{\partial x} \tag{12}$$

Eq. 1 is satisfied, while Eqs 2–4 are transformed as

$$\beta=\left(\frac{b}{\upsilon(1-\alpha t)}\right)^{\frac{1}{2}}h(t) \tag{13}$$

$$\frac{dh}{dt}=\frac{\alpha\beta}{2}\left(\frac{\upsilon}{b(1-\alpha t)}\right)^{\frac{1}{2}} \tag{14}$$

$$\begin{aligned}&\frac{\mu_{hnf}}{\mu_f}\frac{\rho_f}{\rho_{hnf}}f'''-S\left(f'+\frac{\eta}{2}f''\right)-\left(f'\right)^2+ff''+\lambda\left(2ff'f''-f^2f'''\right)-\lambda r\left(f'-\lambda ff''\right)\\ &+\frac{\mu_f}{\mu_{hnf}}M\left[E-\left(f'-\lambda ff''\right)\right]\pm\frac{\beta_{Thnf}}{\beta_f}(Gr\Theta)+\frac{\beta_{Chnf}}{\beta_f}(Gc\Phi)=0,\end{aligned} \tag{15}$$

$$\begin{aligned}&\frac{1}{\Pr}\frac{(\rho Cp)_f}{(\rho Cp)_{hnf}}\left(\frac{k_{hnf}}{k_f}+\frac{4}{3}Rd\right)\Theta''-\frac{S}{2}\left(3\Theta+\eta\Theta'\right)-2f'\Theta+f\Theta'\\ &=0\end{aligned} \tag{16}$$

$$\Phi''+Sc\left(\frac{S}{2}\left(3\Phi+\eta\Phi'\right)-2f'\Phi+f\Phi'\right)-\gamma Sc\Phi=0 \tag{17}$$

$$\left\{\begin{aligned}&S=\frac{\alpha}{a},\lambda=\frac{\lambda_1}{(1-\alpha t)},\lambda_p=\frac{\upsilon}{k^{\oplus}a},\Pr=\frac{\mu Cp}{k},Rd=\frac{4\sigma^* T_h^3}{3k^* k_f(\rho Cp)_{hnf}},\gamma=\frac{Kr}{a},\\ &Gr=\frac{g\beta_{Tf}[T_w-T_h]x^3}{\upsilon_f^2},Gc=\frac{g\beta_C[C_w-C_h]x^3}{\upsilon_f^2}.\end{aligned}\right\} \tag{18}$$

TABLE 1 Thermophysical features of the nanoparticles.

Parameter	APS (average particle size), nm	ρ Kg m^{-3}	k W $m^{-1}k^{-1}$	C_p J $kg^{-1}K^{-1}$
Al_2O_3	25–45	3,970	40	765
Ag	18–23	10,500	429	250
80 wt% Al_2O_3–20 wt% Ag	10–45	2.87	4.768	0.842

where $S, \lambda_p, \Pr, \lambda, \gamma, Gr, Rd, Gc$ are the unsteadiness parameter, porosity term, Prandtl number, Maxwell parameter, chemical reaction, thermal Grashof number, radiation parameter, and mass Grashof number, respectively.

The transform forms of the physical conditions are taken as

$$\left\{\begin{array}{l} f(0) = 0, f'(0) = 1, \Theta(0) = 1, \Phi(0) = 1, \\ f''(\beta) = 0, f(\beta) = \frac{S\beta}{2}, \Theta'(\beta) = 0, \Phi'(\beta) = 0 \end{array}\right\} \tag{19}$$

The skin friction and the local Nusselt and Sherwood numbers are defined as

$$\left.C_f = \frac{2\tau_w}{\rho U_w^2}, N_u = \frac{q_w x}{k(T_w - T_0)}, S_n = \frac{q_m x}{D_B(C_w - C_0)}\right\} \tag{20}$$

where

$$\left.\tau_w = \mu\left(\frac{\partial u}{\partial y}\right)\bigg|_{y=0}, q_w = -k\left(\frac{\partial T}{\partial y}\right)\bigg|_{y=0}, q_m = -D_B\left(\frac{\partial C}{\partial y}\right)\bigg|_{y=0},\right\} \tag{21}$$

The transformed terms are stated as

$$\left.\begin{array}{l} \mathrm{Re}^{\frac{1}{2}} Cf = -\frac{\mu_f}{\mu_{hnf}} f''(0), \quad \mathrm{Re}^{\frac{-1}{2}} Nu = -\left(\frac{k_{hnf}}{k_f} + Rd\right)\Theta'(0), \\ \mathrm{Re}^{\frac{-1}{2}} Sh = -\Phi'(0), \quad \mathrm{Re} = \frac{xU_w}{\upsilon}. \end{array}\right\} \tag{22}$$

Results and discussion

In this section, we display and discuss the results that were computed using the aforementioned technique, HAM. Additionally, as illustrated in Figures 2–17 and Tables 2,Tables 3, the performance of hybrid nanofluid and nanofluid flow $f'(\eta)$, energy $\Theta(\eta)$, and concentration distribution $\Phi(\eta)$ under the impact of fluid parameters is explored. For these purposes, numerical simulations are carried out, with $S = 0.4, \lambda_p = 1, \Pr = 7.5, \lambda = 0.3, \gamma_c = 0.5, Gr = 2, Rd = 0.6, Gc = 1.5$. When the current findings are compared with the previous study of Wang, 1990; Qasim et al., 2016 under limiting circumstances, the validity of the current results is demonstrated. The two sets of results are shown in Tables 2 and 3, and there is considerable agreement between them. According to Table 2, the progressive variation of S is added to the surface and wall temperature gradients.

The characteristics of $f'(\eta)$ (velocity field) and $\Theta(\eta)$ (thermal distributions) in the presence of λ_p (permeability variable) are delineated by Figures 2,3 for nanofluids and hybrid nanofluids. Figure 2 shows that a depletion of $f'(\eta)$ distribution results from increasing λ_p values. This is realistic because a porous medium presents a resistance in the way to fluid flow. Therefore, as demonstrated in Figure 2, high values of the λ_p parameter diminish the fluid velocity. The suspensions of hybrid nanofluids are declined more quickly as compared to monofluids. Additionally, as seen in Figure 3, there is an increase in temperature distributions when the values of the λ_p parameter are improved. Figures 4,5 demonstrate the variations in $f'(\eta)$ (velocity field) and $\Theta(\eta)$ (thermal distributions) with respect to the $\phi_{Al_2O_3}$, ϕ_{Ag} (volume fractions of nanoparticles). Figure 4 shows that the velocity profile appears to decrease when the values of $\phi_{Al_2O_3}$, ϕ_{Ag} nanoparticles grow statistically. In terms of physics, the rise in the values of $\phi_{Al_2O_3}$, ϕ_{Ag} denotes an increase in the number of nanoparticles scattered in the base fluid. The results imply that the minor volume percentage helps the hybrid nanofluid. When compared to ordinary nanofluids, the hybrid suspension achieves a prominent position. According to Figure 5, the $\Theta(\eta)$ distribution improved due to an increase in $\phi_{Al_2O_3}$, ϕ_{Ag}. Physically, the emergence of a greater number of small components into the host liquid makes it easier for the nanoliquids to release a greater quantity of their stored energy in the form of heat. As a result, there was an increase in the effective distribution of heat. Therefore, the hybrid nanofluid achieves a higher level than the typical one. The incorporation of nanocomposites results in an intensification of the process of heat transfer. It is perfectly reasonable because the incorporation of a greater number of nanoparticles into the nanosolution makes it easier to obtain a high rate of heat transmission. Figure 6 illustrates the impact of M (magnetic parameter) on the $f'(\eta)$ field for all cases of nanofluids and hybrid nanofluids. As M is estimated to be a larger value, the velocity of nanofluids decreases. Because an increase in M signifies an improvement in resistive force (the Lorentz force), this results in a reduction in the velocity of the nanofluid and hybrid nanoliquid. According to Figure 7, a higher E value results in an improved $f'(\eta)$ field. This is due to the fact that an increase in E contributes to the

TABLE 2 Comparison between the published work and present work for the surface and wall temperature gradients considering common factors using the regular fluid having Pr = 7.56. Note that they used small and variable values of the Prandtl number.

	Wang (1990)	Wang (1990)	Qasim et al. (2016)	Qasim et al. (2016)	Present	Present
S	$\Theta(1)$	$-\Theta'(0)$	$\Theta(\beta)$	$-\beta\Theta'(0)$	$\Theta(\beta)$	$-\beta\Theta'(0)$
0.3	0.45312	0.6413	0.45921	0.64374	0.4594251	0.64365
0.5	0.47683	0.7658	0.47941	0.76832	0.4794732	0.768320
0.7	0.49587	0.8513	0.49926	0.85383	0.4992763	0.853241
0.9	0.51325	0.9924	0.51732	0.51823	0.517276	0.5172751

TABLE 3 Comparison between the published work and present work for the Sherwood number considering the common factor using the regular fluid having Pr = 7.56, S = 0.8.

	Qasim et al. (2016)	Qasim et al. (2016)	Present	Present
Sc	$\Phi(\beta)$	$-\Phi'(0)$	$\Phi(\beta)$	$-\Phi'(0)$
9	0.13743	0.4587	0.137563	0.458872
11	0.129341	0.44575	0.129432	0.445834
13	0.11832	0.42782	0.11843	0.427942

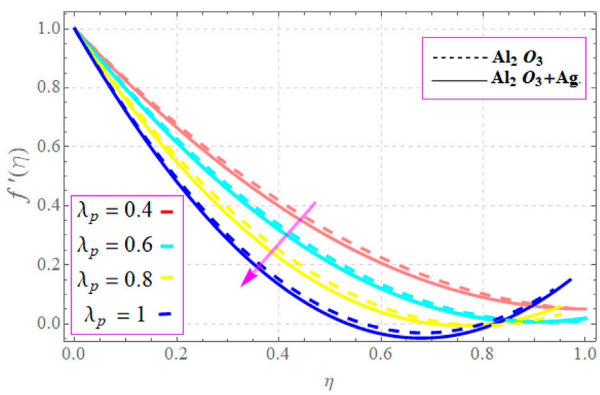

FIGURE 2
λ_p vs $f'(\eta)$.

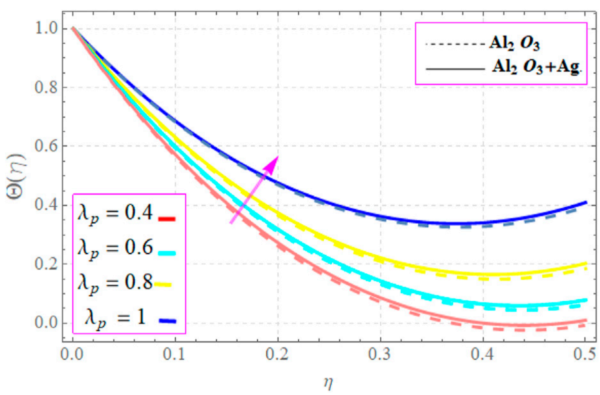

FIGURE 3
Influence of λ_p on $\Theta(\eta)$.

generation of a stronger electric field, which in turn speeds up the flow of nanofluids and hybrid nanofluids. The characteristics of the flow field $f'(\eta)$ for different values of Gr and Gc (thermal and mass buoyancy parameters) are shown in Figures 8, 9. Figure 8 illustrates the unique effects of Gr on the resulting velocity. The $f'(\eta)$ of the thin-film fluid increases as Gr rises. Actually, Gr is the ratio of thermal buoyant forces to viscous forces. As a consequence, the strengths of thermal forces rise as the magnitude of Gr increases. Huge quantities of the Grashof number are used to provide the buoyancy forces. Thus, as Gr rises, the resulting momentum boundary layer's thickness also rises. The special impact of Gc on the fluid velocity $f'(\eta)$ is shown in Figure 9. As the Gc increases, the $f'(\eta)$ of the hybrid thin-film fluid also increases. The Gc is the proportionality of concentration buoyant forces to viscous forces. The intensities of solutal force increase as the magnitude of the Gc increases. Also, when compared to ordinary nanofluids, the hybrid suspension achieves a prominent position.

The changes in the $\Theta(\eta)$ profile relative to the Rd (radiation parameter) are shown in Figure 10 for nanofluids and hybrid nanofluids. It is considered that an elevation in Rd factor leads the temperature to rise. Physically, the Rd factor compares the input of heat exchange through conduction to transfer using thermal

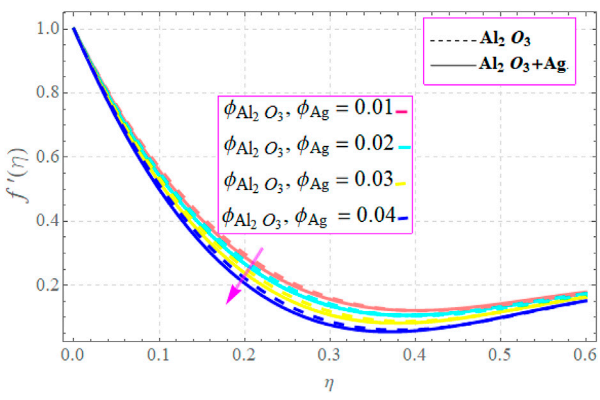

FIGURE 4
Influence of $\phi_{Al_2O_3}$, ϕ_{Ag} on $f'(\eta)$.

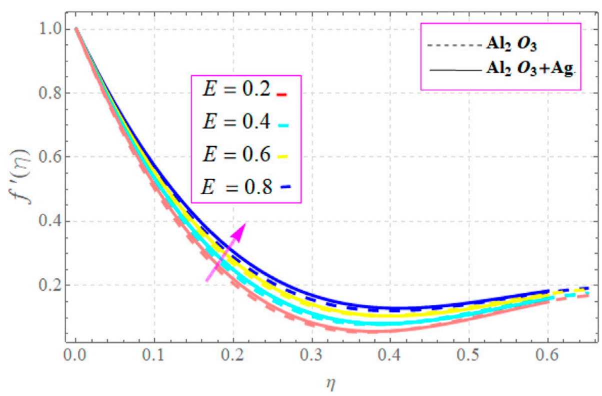

FIGURE 7
Influence of E on $f'(\eta)$.

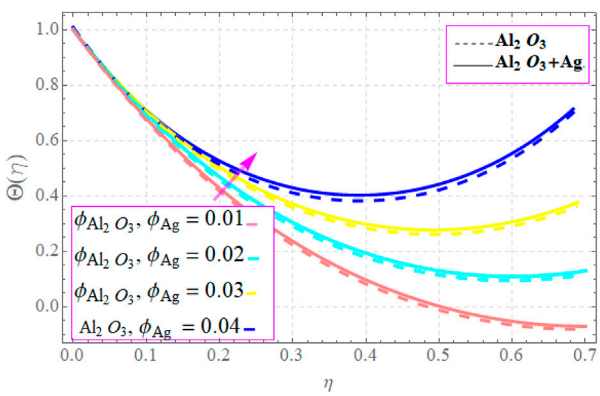

FIGURE 5
Influence of $\phi_{Al_2O_3}$, ϕ_{Ag} on $\Theta(\eta)$.

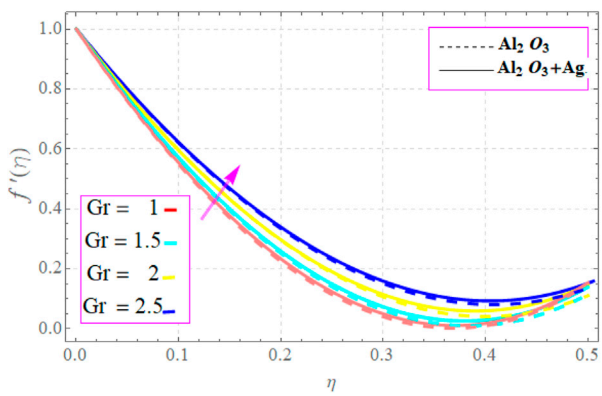

FIGURE 8
Influence of Gr on $f'(\eta)$.

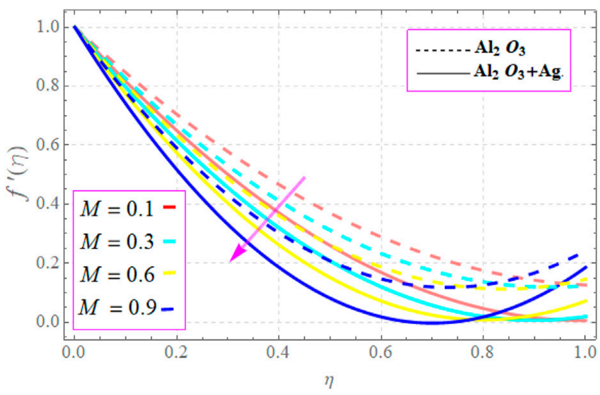

FIGURE 6
Influence of M on $f'(\eta)$.

radiation. It is obvious that an increase in the radiation parameter causes the temperature to rise. Additionally, there is a positive association between the Rd and the temperature gradient close to the surface of the plate. Hence, the hybrid nanofluid shows the leading nature as compared to the nanofluid. The effect of S (unsteadiness factor) on the $f'(\eta)$ profile is shown in Figure 11 for nanofluids and hybrid nanofluids. The plot reveals that a gradual increase in the magnitude of S causes the $f'(\eta)$ profile to gradually decline, improving the momentum boundary film viscosity. The hybrid suspension also holds a prominent position when compared to regular nanofluids. Figure 12 predicts the significance of the $\Theta(\eta)$ distribution on the S (unsteadiness factor) for both the types of nanofluids and hybrid nanofluids. It is important to note that S has an increasing impact on the temperature of the liquid film. A slight temperature improvement is shown to increase the values of S in the boundary layer.

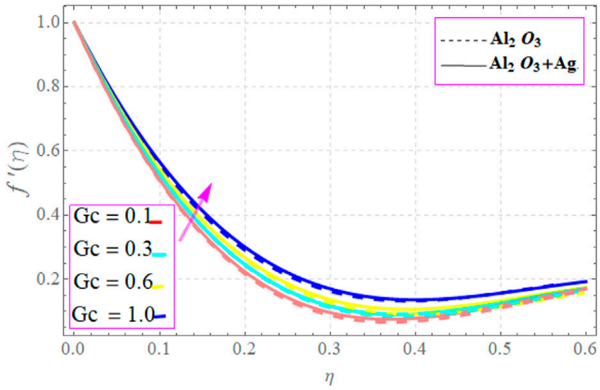

FIGURE 9
Influence of *Gc* on $f'(\eta)$.

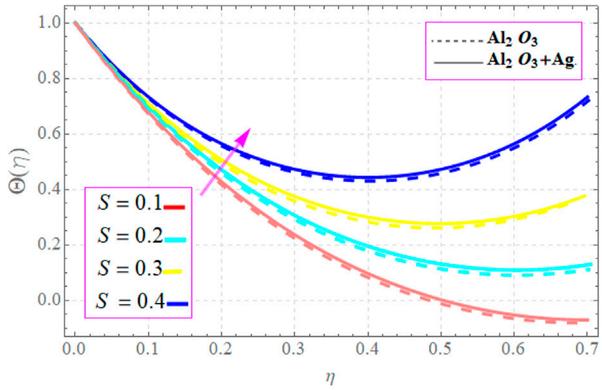

FIGURE 12
Influence of *S* on $\Theta(\eta)$.

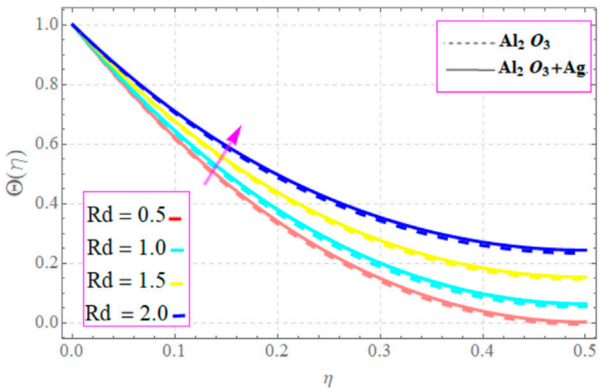

FIGURE 10
Influence of *Rd* on $\Theta(\eta)$.

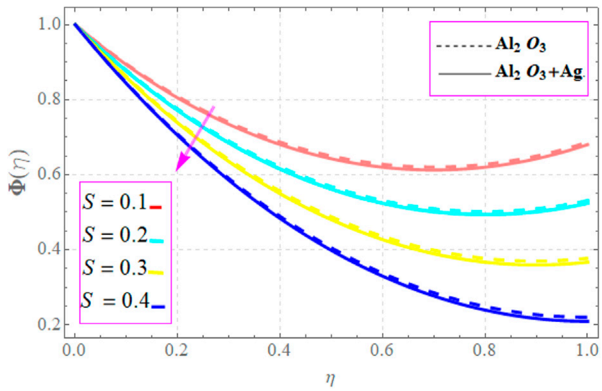

FIGURE 13
Influence of *S* on $\Phi(\eta)$.

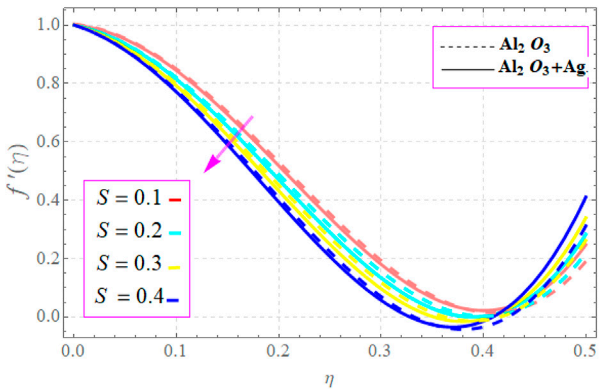

FIGURE 11
Influence of *S* on $f'(\eta)$.

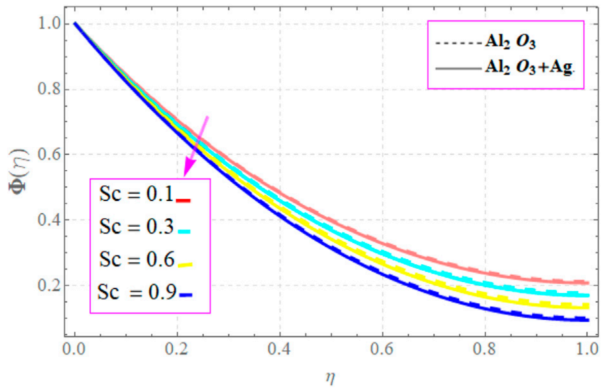

FIGURE 14
Influence of *Sc* on $\Phi(\eta)$.

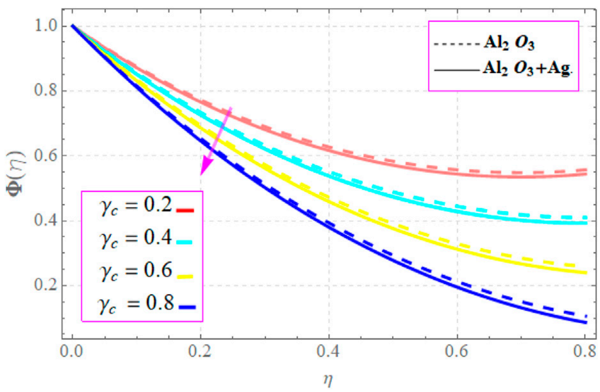

FIGURE 15
Influence of γ_c on $\Phi(\eta)$.

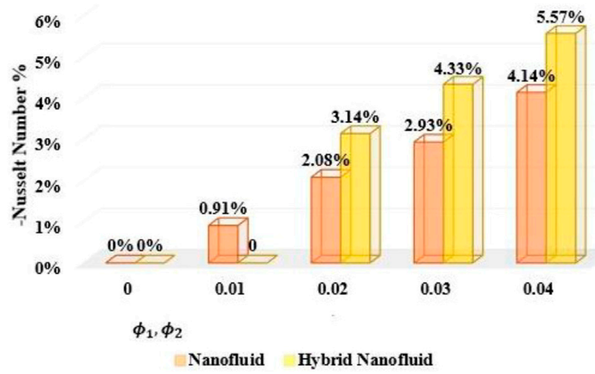

FIGURE 18
ϕ_1, ϕ_2 vs Nusselt number enhancement in %.

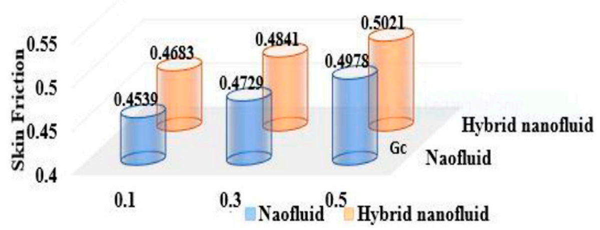

FIGURE 16
Gc vs skin friction.

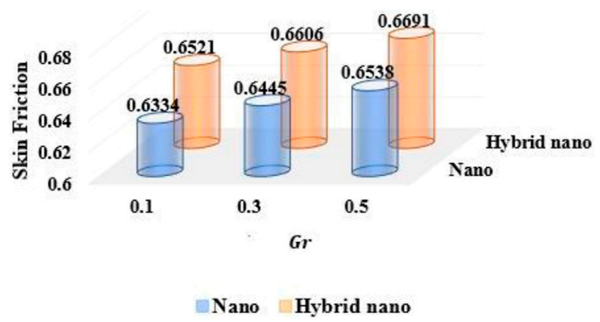

FIGURE 17
Gr vs skin friction.

Figure 13 illustrates how the presence of S changed the $\Phi(\eta)$ concentration profile for both types of nanofluids. The tendency occurs for the liquid to be pushed into empty spaces as a result of the enhancement of S. As a result, the $\Phi(\eta)$ increases, as depicted in Figure 13, for both the Al_2O_3 and Al_2O_3-Ag nanosolutions. Plot Figure 14 illustrates the significance of Sc (Schmidt number) in regard to the $\Phi(\eta)$ profile for nanofluids and hybrid nanofluids. As Sc increases, a noticeable lowering of the $\Phi(\eta)$ distribution can be seen. According to its definition, Sc is the ratio of the momentum diffusivity to the mass diffusivity. Therefore, more species (higher Sc) depreciate the solutal fields. The behavior of the dimensionless $\Phi(\eta)$ distribution for various values in γ_c (chemical reactions) is depicted in Figure 15 for the cases of nanofluids and hybrid nanofluids. In this study, $\gamma_c > 0$, and the effects of destructive chemical reactions are investigated. The plot shows a decrease in the $\Phi(\eta)$ field as γ_c rises. Physically, high values of the γ_c parameter indicate that there are many solute molecules taking part in the reaction, which causes the $\Phi(\eta)$ field to drop. As a result, a destructive chemical reaction dramatically reduces the thickness of the solutal border layer. Also, when compared to the Al_2O_3 nanofluid, the Al_2O_3-Ag suspension achieves a prominent position. Figures 16, 17 show the variation of the skin friction coefficient for different values of Gc and Gr for nanofluids and hybrid nanofluids. Also, the consequences of ϕ_1, ϕ_2 against Nusselt number enhancement in % age are presented in Figures 18.

Conclusion

We focused on describing the chemical radiative and convectional effects on the hydrothermal characteristics of two different types of Maxwell nanoliquids, the Ag hybrid nanofluid and Al_2O_3 regular nanofluid, during the entire study. Over a permeable stretched inclined surface, the desired thin-film flow has been passed. Through tables and figures, exhaustive properties of porosity, volume fraction, unsteadiness, radiation, chemical reaction, and thermal and mass buoyancy components are explained. Through a comprehensive examination, some guiding points help focus our attention on the following findings:

- Maxwell hybrid nanofluids' thin-film flow is slowed down by increased λ_p (porosity).
- $\phi_{Al_2O_3}$, ϕ_{Ag} (nanoparticle volume fraction), S (unsteadiness), Gr, and Gc (Thermal and mass buoyancy parameters) parameters highly influence the thin-film flow of Maxwell hybrid nanofluids compared to nanofluids.
- For the thermal profile, $\phi_{Al_2O_3}$, ϕ_{Ag} (nanoparticle volume fraction), S (unsteadiness), and λ_p (porosity) have similar effects. These factors have a greater impact on hybrid nanofluids than on nanofluids.
- For the concentration profile, the thin film of the hybrid fluid is more influenced than the nanofluid by S as compared to the other various parameters like Sc and γ_c.
- The skin friction coefficient, Nusselt number, and Sherwood number reduce when uplifting the parameter S, while it increases for $\phi_{Al_2O_3}$, ϕ_{Ag}, and λ_p.

Future direction

These results of thin-film flows can also be used for other models like discs and cylinders, different flow factors, and trihybrid nanofluids with the execution of numerical and analytical techniques.

Data availability statement

The raw data supporting the conclusions of this article will be made available by the authors, without undue reservation.

Author contributions

TG, modeling and solution; SM, writing draft WA, editing. ETE, Validated, MFY and KG, participated in revision and provide funding source.

Funding

The authors would like to thank the Deanship of Scientific Research at Umm Al-Qura University for supporting this work by Grant Code: (22UQU4331317DSR78).

Conflict of interest

The authors declare that the research was conducted in the absence of any commercial or financial relationships that could be construed as a potential conflict of interest.

Publisher's note

All claims expressed in this article are solely those of the authors and do not necessarily represent those of their affiliated organizations or those of the publisher, the editors, and the reviewers. Any product that may be evaluated in this article or claim that may be made by its manufacturer is not guaranteed or endorsed by the publisher.

References

Abro, K. A., Soomro, M., Atangana, A., and Gómez-Aguilar, J. F. (2020). Thermophysical properties of Maxwell nanofluids via fractional derivatives with regular kernel. *J. Therm. Analysis Calorim.* 147, 1–11. doi:10.1007/s10973-020-10287-9

Acharya, N., Maity, S., and Kundu, P. K. (2020). Influence of inclined magnetic field on the flow of condensed nanomaterial over a slippery surface: The hybrid visualization. *Appl. Nanosci.* 10 (2), 633–647. doi:10.1007/s13204-019-01123-0

Ahmed, J., Khan, M., and Ahmad, L. (2020). Radiative heat flux effect in flow of Maxwell nanofluid over a spiraling disk with chemically reaction. *Phys. A Stat. Mech. its Appl.* 551, 123948. doi:10.1016/j.physa.2019.123948

Ali, L., Liu, X., and Ali, B. (2020). Finite element analysis of variable viscosity impact on MHD flow and heat transfer of nanofluid using the cattaneo-christov model. *Coatings* 10 (4), 395. doi:10.3390/coatings10040395

Ayub, A., Sabir, Z., Altamirano, G. C., Sadat, R., and Ali, M. R. (2021). Characteristics of melting heat transport of blood with time-dependent cross-nanofluid model using Keller–Box and BVP4C method. *Eng. Comput.* 1, 1–15.

Ayub, A., Wahab, H. A., Shah, S. Z., Shah, S. L., Darvesh, A., Haider, A., et al. (2021). Interpretation of infinite shear rate viscosity and a nonuniform heat sink/source on a 3D radiative cross nanofluid with buoyancy assisting/opposing flow. *Heat. Transf.* 50 (5), 4192–4232. doi:10.1002/htj.22071

Babar, H., and Ali, H. M. (2019). Towards hybrid nanofluids: Preparation, thermophysical properties, applications, and challenges. *J. Mol. Liq.* 281, 598–633. doi:10.1016/j.molliq.2019.02.102

Choi, S. U. S. (1995). Enhancing thermal conductivity of fluids with nanoparticles. *ASME-Publications-Fed* 231, 99–106.

Devi, S. A., and Devi, S. S. U. (2016). Numerical investigation of hydromagnetic hybrid Cu - Al2O3/water nanofluid flow over a permeable stretching sheet with suction. *Int. J. Nonlinear Sci. Numer. Simul.* 17 (5), 249–257. doi:10.1515/ijnsns-2016-0037

Ghadikolaei, S. S., Hosseinzadeh, K., Ganji, D. D., and Jafari, B. (2018). Nonlinear thermal radiation effect on magneto Casson nanofluid flow with Joule heating effect over an inclined porous stretching sheet. *Case Stud. Therm. Eng.* 12, 176–187. doi:10.1016/j.csite.2018.04.009

Gumber, P., Yaseen, M., Rawat, S. K., and Kumar, M. (2022). Heat transfer in micropolar hybrid nanofluid flow past a vertical plate in the presence of thermal radiation and suction/injection effects. *Partial Differ. Equations Appl. Math.* 5, 100240. doi:10.1016/j.padiff.2021.100240

Hussain, S. M., Sharma, R., Mishra, M. R., and Alrashidy, S. S. (2020). Hydromagnetic dissipative and radiative graphene Maxwell nanofluid flow past a stretched sheet-numerical and statistical analysis. *Mathematics* 8 (11), 1929. doi:10.3390/math8111929

Jawad, M., Saeed, A., and Gul, T. (2021). Entropy generation for MHD Maxwell nanofluid flow past a porous and stretching surface with Dufour and Soret effects. *Braz J. Phys.* 51 (3), 469–480. doi:10.1007/s13538-020-00835-x

Jeffreys, H. (1925). LIV. The flow of water in an inclined channel of rectangular section. *Lond. Edinb. Dublin Philosophical Mag. J. Sci.* 49 (293), 793–807. doi:10.1080/14786442508634662

Joshi, N., Upreti, H., and Pandey, A. K. (2022). MHD Darcy-Forchheimer Cu-Ag/H2O-C2H6O2 hybrid nanofluid flow via a porous stretching sheet with suction/blowing and viscous dissipation. *Int. J. Comput. Methods Eng. Sci. Mech.* 1, 1–9.

Khan, S. U., Rauf, A., Shehzad, S. A., Abbas, Z., and Javed, T. (2019). Study of bioconvection flow in Oldroyd-B nanofluid with motile organisms and effective Prandtl approach. *Phys. A Stat. Mech. its Appl.* 527, 121179. doi:10.1016/j.physa.2019.121179

Khan, S. U., and Shehzad, S. A. (2020). Flow of Jeffrey nanofluids over convectively heated oscillatory moving sheet with magnetic field and porosity effects. *J. Por Media* 23 (9), 907–922. doi:10.1615/jpormedia.2020025508

Khan, S. U., Shehzad, S. A., Rauf, A., and Abbas, Z. (2020). Thermally developed unsteady viscoelastic micropolar nanofluid with modified heat/mass fluxes: A generalized model. *Phys. A Stat. Mech. its Appl.* 550, 123986. doi:10.1016/j.physa.2019.123986

Liu, Y., Itoh, M., and Kyotoh, H. (2017). Flow of a falling liquid curtain onto a moving substrate. *Fluid Dyn. Res.* 49 (5), 055501. doi:10.1088/1873-7005/aa7ee8

Nadeem, S., Israr-ur-Rehman, M., Saleem, S., and Bonyah, E. (2020). Dual solutions in MHD stagnation point flow of nanofluid induced by porous stretching/shrinking sheet with anisotropic slip. *AIP Adv.* 10 (6), 065207. doi:10.1063/5.0008756

Nusselt, W. (1916). Die oberflachenkondensation des wasserdamphes. *VDI-Zs* 60, 541.

Qasim, M., Khan, Z. H., Lopez, R. J., and Khan, W. A. (2016). Heat and mass transfer in nanofluid thin film over an unsteady stretching sheet using Buongiorno's model. *Eur. Phys. J. Plus* 131 (1), 1–11. doi:10.1140/epjp/i2016-16016-8

Ramesh, K., Khan, S. U., Jameel, M., Khan, M. I., Chu, Y. M., and Kadry, S. (2020). Bioconvection assessment in Maxwell nanofluid configured by a Riga surface with nonlinear thermal radiation and activation energy. *Surfaces Interfaces* 21, 100749. doi:10.1016/j.surfin.2020.100749

Sabir, Z., Akhtar, R., Zhiyu, Z., Umar, M., Imran, A., Wahab, H. A., et al. (2019). A computational analysis of two-phase casson nanofluid passing a stretching sheet using chemical reactions and gyrotactic microorganisms. *Math. Problems Eng.* 2019, 1–12. doi:10.1155/2019/1490571

Sabir, Z., Imran, A., Umar, M., Zeb, M., Shoaib, M., and Raja, M. A. Z. (2021). A numerical approach for 2-D Sutterby fluid-flow bounded at a stagnation point with an inclined magnetic field and thermal radiation impacts. *Therm. Sci.* 25 (3), 1975–1987.

Shah, S. A., Mouldi, A., and Sene, N. (2022). Nonlinear convective SiO2 and TiO2 hybrid nanofluid flow over an inclined stretched surface. *J. Nanomater.* 2022, 1–15.

Sharma, R., Hussain, S. M., Raju, C. S. K., Seth, G. S., and Chamkha, A. J. (2020). Study of graphene Maxwell nanofluid flow past a linearly stretched sheet: A numerical and statistical approach. *Chin. J. Phys.* 68, 671–683. doi:10.1016/j.cjph.2020.10.013

Turkyilmazoglu, M. (2020). Single phase nanofluids in fluid mechanics and their hydrodynamic linear stability analysis. *Comput. Methods Programs Biomed.* 187, 105171. doi:10.1016/j.cmpb.2019.105171

Umar, M., Sabir, Z., Imran, A., Wahab, A. H., Shoaib, M., and Raja, M. A. Z. (2020). The 3-D flow of Casson nanofluid over a stretched sheet with chemical reactions, velocity slip, thermal radiation and Brownian motion. *Therm. Sci.* 24 (5), 2929–2939. doi:10.2298/tsci190625339u

Wang, C. Y. (1990). Liquid film on an unsteady stretching surface. *Quart. Appl. Math.* 48 (4), 601–610. doi:10.1090/qam/1079908

Yaseen, M., Rawat, S. K., and Kumar, M. (2022). Hybrid nanofluid (MoS 2 -SiO 2/water) flow with viscous dissipation and Ohmic heating on an irregular variably thick convex/concave-shaped sheet in a porous medium. *Heat. Trans.* 51 (1), 789–817. doi:10.1002/htj.22330

Zhang, Y., Shahmir, N., Ramzan, M., Ghazwani, H. A. S., and Malik, M. Y. (2021). Comparative analysis of Maxwell and Xue models for a hybrid nanofluid film flow on an inclined moving substrate. *Case Stud. Therm. Eng.* 28, 101598. doi:10.1016/j.csite.2021.101598

10.3389/fenrg.2022.970293

Nomenclature

λ_1 relaxation time

τ tensor for extra stress

κ thermal conductivity

C_p heat capacitance

η similarity variable

T_0, T_{ref} temperature terms

S unstable parameter

T temperature

υ_{hnf}, kinematic viscosity

u, v velocity components

ρ density

μ_{hnf} dynamic viscosity of the hybrid nanofluid

Sc Schmitt number

$k^{\oplus}$ permeability coefficient

λ time relaxation

Pr Prandtl number

Θ dimensionless temperature

$h(t)$ film thickness